Influence of Rigid/Deformable Foil Shape on the Hydrodynamic Loads and Performance

Huili Xu[1,*], Marilena Greco[1,2], Claudio Lugni[1,2]
[1]Centre for Autonomous Marine Operations and System (AMOS), Department of Marine Technology, NTNU, Trondheim, Norway
[2]CNR-INM, Institute of Marine Engineering, Rome, Italy
hui-li.xu@ntnu.no

1 INTRODUCTION

Many swimming fishes can be considered as underwater bio vehicles with high hydrodynamic efficiency and performance, such as low resistance, high speed, and good maneuverability. The basis source of their propulsion forces is the control of vortices produced by their oscillating bodies and fins. Inspired by fish, the thrust-producing harmonically oscillating foils have been studied extensively through both experimental and numerical techniques. In the present work, various two-dimensional (2D) flapping foils are studied with focus on the influence of rigid and deformable fish-like profiles on the hydrodynamic loads and performance. Herein, a morphing strategy of the foil is pursued to combine the advantages of the rigid foils with different shapes, that is, to maximize the thrust and efficiency while minimizing the required mean input power during pitching motion.

2 MODELLING AND METHODOLOGY

In order to understand better the flapping performances of foils with different profiles in a proper manner, three symmetric hydrofoils with the same chord length c are examined, as shown in fig. 1.

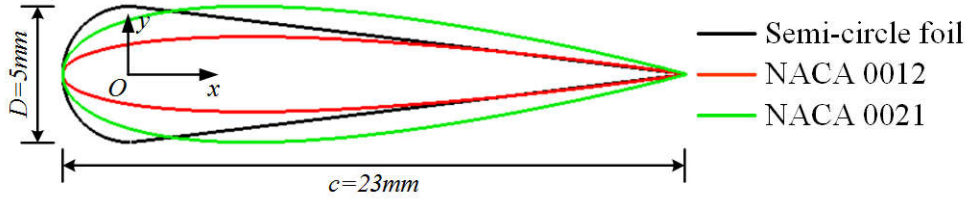

Figure 1: Schematic view of the examined fish-like foil profiles

The tear-shaped foil with a semicircular leading edge and a triangular form in the aft is adopted from a reference experiment [1]. The trailing edge of NACA 0012 foil is as sharp as the semi-circle foil, but its maximum thickness D is ~43% smaller. In contrast, we selected NACA 0021 foil that has the same maximum thickness as the semi-circle foil, but it is thicker in the aft part. Each foil was studied in the following scenario: placed in a uniform current with constant inflow speed U in the horizontal direction parallel to the x-axis and forced to perform pitching motions (about O and z-axis). The angular motions are described by $\theta(t) = \theta_0 \sin(\omega t)$. Here $\omega = 2\pi f$ is the angular frequency, and θ_0 is the maximum pitching angle. During the prescribed motion, the foil is aligned with the inflow at $\omega t = n\pi$ (with $n = 1,2,\dots$) and reaches the extreme inclined positions at $\omega t = n\pi + \pi/2$ (maximum rotation to the top) and $n\pi + 3\pi/2$ (maximum rotation to the bottom). In this work, the foils are studied with the following parameters: $f = 2.244s^{-1}$, $\theta_0 = 0.153rad$ (i.e., peak-to-peak amplitude at the trailing edge $A = 6.25mm$) and the chord-based Reynolds number, $Re = Uc/\nu$ (ν is the kinematic viscosity of fluid), is set as $Re = 1173$, i.e., consistent with the reference experimental study where quasi-2D mechanisms in the fluid-body interactions are documented.

The simulations are performed as 2D within a stepwise research strategy and using a thoroughly validated finite-volume-based code in the OpenFOAM platform based on a collocated grid. The

PIMPLE algorithm is employed for solving the incompressible Navier-Stokes equations, which combines PISO (Pressure Implicit with Splitting of Operator) and SIMPLE (Semi-Implicit Method for Pressure Linked Equations) algorithms. A second-order scheme is used for the space discretization, and the implicit Euler scheme is chosen for the time discretization as compromise between numerical accuracy and computational cost. To handle the large motions of pitching foil, the overset grid method is employed in this work [2]. The computational domain around the flapping foil is defined by a rectangle extending 5.2 chords upstream and 6.5 chords downstream. The domain transverse dimension is $-3.26c < y < 3.26c$, which is the same as the tunnel width in the reference experiment. Detailed boundary conditions are shown in fig. 2 and numerical-convergence analysis for this hydrodynamic problem can be found in [3]. Due to the linear interpolation between grids in openFOAM, the overset mesh is constructed so that the outermost layer of the moving mesh has comparable cell size as the background grid. Therefore, the employed grid has 3640 hexahedral cells in the overset region and 288000 structured cells for the background mesh.

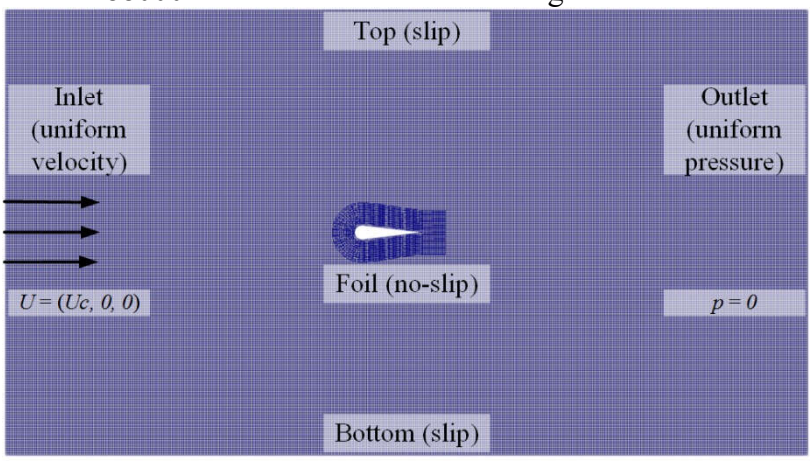

Figure 2: Computational domain and boundary conditions for the flapping foil

Additionally, all simulations are run on supercomputer VILJE nodes (Intel Xeon E5-2670) using 2 nodes (32 cores) per simulation and FRAM nodes (Intel E5-2683v4 2.1 GHz) with 1 node (32 cores) per simulation.

3 INFLUENCE OF RIGID FOIL SHAPE

The investigations of the three rigid foils focus on their thrust force F_x, input power requirement P and propulsion efficiency η. The corresponding nondimensional coefficients are defined, respectively, as $C_x = F_x/0.5\rho U^2 c$, $C_P = P/0.5\rho U^3 c$, and $\eta = F_x U/P = C_x/C_P$. Here ρ is the density of the fluid, P is the mechanical power required to activate the foil, calculated as $P = M_z\dot{\theta}$, with M_z the hydrodynamic torque. Based on the above definitions, the foil experiences thrust when $C_x < 0$ and requires input power when $C_P < 0$.

The steady-state behaviors of horizontal-force and power coefficients within one complete oscillation period for the three rigid hydrofoils are shown in fig. 3. Under the aforementioned conditions, the NACA 0012 and NACA 0021 foils are associated with thrust generation and drag generation, respectively, and the semi-circle foil is at the drag-thrust transition. C_x and C_P in the three cases are periodic with a period half of the pitching period, which is expected due to the symmetry of the foils and of their rotational motion with respect to the x-axis. Their extreme values occur nearly at the same phases ωt; this is exactly true for C_P and nearly true for C_x. In addition, the inflection points of the C_P curve practically synchronize with the extremes of the C_x curve, i.e., maximum instantaneous thrust/drag force. However, there are obvious differences among the results of the three foils. From the plots, the C_x curves for the NACA 0012 and semi-circle foils have similar oscillation amplitude,

while the one for the NACA 0021 foil has a slightly smaller value. This indicates that the force oscillation amplitude is dominated by mechanisms connected with the shape of the trailing edge and increases for sharper/thinner geometries. Besides, the NACA 0021 and semi-circle foils experience similar maximum drag (positive C_x), occurring slightly after the foil has passed its mean position, while the NACA 0012 foil has a smaller maximum drag; this confirms the primary role of the maximum thickness in the forward part of the foil for this force contribution. The C_P histories of the semi-circle foil and NACA 0012 foil practically coincide. The NACA 0021 foil has the same maximum C_P, but its minimum value at $\omega t = 7\pi/8$ has a smaller magnitude than that documented by the other two foils. Because the pitching frequency and amplitude are the same, the only reason for this is the torque experienced by the hydrofoils, as shown in the right plot of fig. 3. When the foils move from the extreme positions to the mean positions, the torque for NACA 0021 foil becomes smaller than for the other foils. This confirms the importance of the trailing edge shape in this case, and highlights that a thicker trailing edge leads to lower input power requirement. The influence of the foil shape can also be studied from the analysis on the pressure and friction components of the hydrodynamic force.

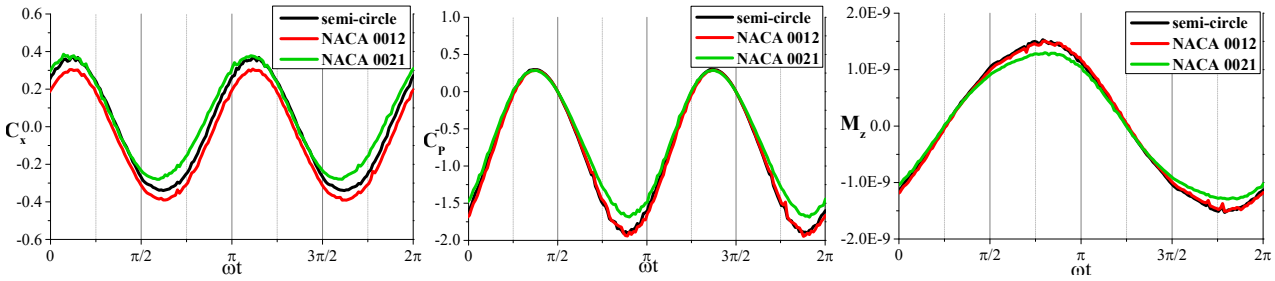

Figure 3: Steady-state horizontal force and input power coefficients and torque for the three rigid foils

4 INFLUENCE OF DEFORMABLE FOIL SHAPE

The analysis of the rigid flapping foils showed that the NACA 0012 foil is associated to the largest thrust but experiences the largest hydrodynamic torque, which might pose possible issues for robustness. This leads to the following research question: can we identify a morphing-foil strategy so to generate a thrust similar to that of the NACA 0012 foil while reducing the hydrodynamic torque to a level comparable to that of the NACA 0021 foil?

A first attempt to combine these advantages within a foil morphing strategy is to enforce that the foil becomes thicker when close to the mean position and thinner when close to the extreme positions. Therefore, the thickness of the foil profile is forced to change in time according to the law: $D(t) = D_0 + D_1(t) = D_0 + a_D(\cos(2\omega t + \phi) - 1)$, with D_0 the mean value and $D_1(t)$ the oscillating part with an amplitude a_D, a period half of the pitching period and a phase ϕ with respect to the pitching motion of the foil, set to zero as first attempt. To pursue our scope, the deformation parameters are chosen so to ensure that the foil profile is morphed between the NACA 0012 and NACA 0021 foils, as illustrated in fig. 4.

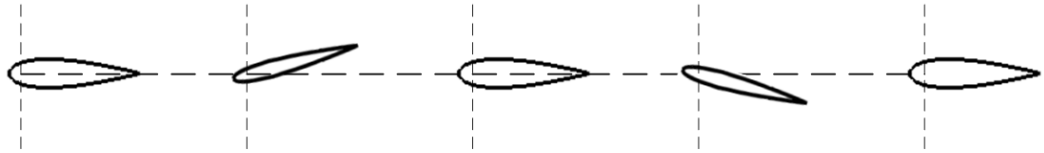

Figure 4: Schematic showing foil morphing between NACA 0012 and 0021 during one oscillation period

This deformable NACA foil is studied under the same pitching condition as for the rigid cases ($f = 2.244s^{-1}$ and $\theta_0 = 0.153rad$). Fig. 5 compares the horizontal force and power from the rigid and

deformable NACA foils. From the plots of C_x, the horizontal force for the deformable NACA foil is not in phase with those for the rigid foils. The deformable NACA foil generates the maximum thrust force (minimum C_x) at the extreme positions and experiences the largest drag just before reaching the mean positions. Its minimum C_x value is the same as for the blunt NACA 0021 foil, however, its maximum C_x value is even smaller than that for the streamlined NACA 0012 foil. Therefore, the deformable NACA foil generates a time-averaged thrust force, which is slightly smaller than that of the NACA 0012 foil, while the NACA 0021 foil suffers a mean drag. The time histories of C_P prove that the deformable NACA foil requires as less power as NACA 0021 foil to perform the prescribed pitching motion.

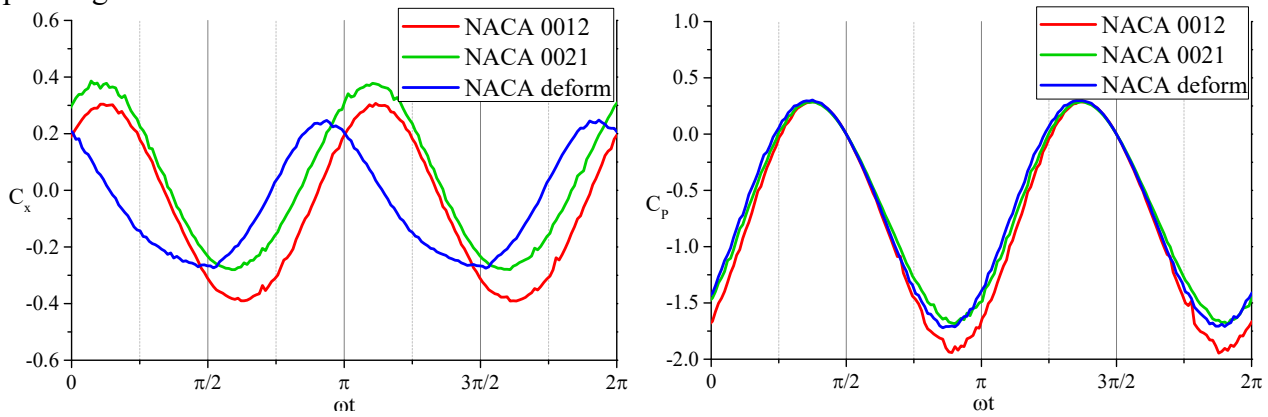

Figure 5: Steady-state horizontal force and input power coefficients for rigid and deformable NACA foils

This attempt proves that a morphing strategy could serve to our scope. This brings to the next research question: is it possible to identify an optimized morphing strategy so to maximize the mean thrust and efficiency while minimizing the required mean input power? To answer to this question, the phase ϕ has been systematically changed while keeping the other deformation parameters unchanged. The results of such investigation will be presented in the workshop.

5 CONCLUSIONS

Three rigid foils with different profiles and a series of deformable foils are studied under the same flapping conditions to investigate the influence of rigid/deformable foil shape on the hydrodynamic loads and performances. Here, a morphing-foil strategy based on the NACA 0012 and NACA 0021 foils is proposed and developed in the OpenFOAM platform to combine the advantages of the rigid foils. The results support that this strategy could enable to achieve large thrust force and high efficiency while reducing the requirement for input power.

ACKNOWLEDGEMENT

The work is sponsored by the Research Council of Norway through the Centre of Excellence funding scheme, project number 223254, AMOS. The simulations were performed on resources provided by UNINETT Sigma2 - the National Infrastructure for High Performance Computing and Data Storage in Norway.

REFERENCES

[1] Godoy-Diana, R., Aider, J. L., & Wesfreid, J. E., 2008. *Transitions in the wake of a flapping foil*. Phys. Rev. E, 77(1), 016308.

[2] Siddiqui, M. A., Xu, H. L., Greco, M., & Colicchio, G., 2020. *Analysis of Open-Source CFD Tools for Simulating Complex Hydrodynamic Problems*. In International Conference on Offshore Mechanics and Arctic Engineering (Vol. 84409, p. V008T08A036). American Society of Mechanical Engineers..

[3] Xu, H. L., Greco, M., & Lugni, C., 2021. *2D Numerical Study on Wake Scenarios for a Flapping Foil*. In International Conference on Offshore Mechanics and Arctic Engineering (Vol. 85185, p. V008T08A033). American Society of Mechanical Engineers.